Improving MR Quantification of Regional Blood Volume with Intravascular T_1 Contrast Agents: Accuracy, Precision, and Water Exchange

Kathleen M. Donahue, Robert M. Weisskoff, David A. Chesler, Kenneth K. Kwong, Alexei A. Bogdanov, Jr., Joseph B. Mandeville, Bruce R. Rosen

The goal of this work was to develop a comprehensive understanding of the relationship between vascular proton exchange rates and the accuracy and precision of tissue blood volume estimates using intravascular T_1 contrast agents. Using computer simulations, the effects of vascular proton exchange and experimental pulse sequence parameters on measurement accuracy were quantified. T_1 and signal measurements made in a rat model implanted with R3230 mammary adenocarcinoma tumors demonstrated that the theoretical findings are biologically relevant; data demonstrated that over-simplified exchange models may result in measures of tumor, muscle, and liver blood volume fractions that depend on experimental parameters such as the vascular contrast concentration. As a solution to the measurement of blood volume in tissues with exchange that is unknown, methods that minimize exchange rate dependence were examined. Simulations that estimated both the accuracy and precision of such methods indicated that both the inversion recovery and the transverse-spoiled gradient echo methods using a "no-exchange" model provide the best trade-off between accuracy and precision.

Key words: blood volume; vascular proton exchange; angiogenesis; intravascular contrast agents.

INTRODUCTION

Tissue blood volume changes are seen in response to functional challenges such as photic stimulation (1), and in response to a variety of disease processes including cerebral, myocardial, and renal ischemia (2, 3) and with tumor angiogenesis (4). In analogy with nuclear medicine techniques, numerous MRI studies have been undertaken to evaluate tissue blood volume fraction with long-lived intravascular T_1 contrast agents. However, unlike nuclear medicine techniques, the MR signal intensity is not a direct measure of contrast concentration. Rather, it is a measure of the effect that the agent has on proton relaxation. Therefore, although an agent may be confined to a given compartment, its effect can extend to other compartments via proton (water) exchange. Consequently, interpretation of MRI studies, which use intravascular T_1 contrast agents, are made more complex by the water exchange that takes place between the vascular and extravascular spaces. In practice the issue of vascular-extravascular proton exchange is taken into account by determining the fractional blood volume in one of two limits of water exchange: from the T_1 relaxation rate assuming fast proton exchange (5–7) or MR signal intensity differences assuming no proton exchange (3, 8) between the vascular and extravascular spaces. The degree to which these conditions are satisfied depends on the relative values of the exchange rate (a physiologic parameter) and the compartmental relaxation rates that can be altered by contrast concentration (an experimental parameter). However, recent results indicate that for typical doses of contrast agent, the vascular proton exchange rate in brain and cardiac tissue is not fast and possibly intermediate relative to the compartmental T_1 relaxation rates (9–12). Consequently, it is questionable as to whether the simple exchange models can be used to accurately measure blood volume.

The goal of this work was to develop a more comprehensive understanding of measurement and exchange parameters as they relate to the measurement of blood volume. This goal is addressed in four main parts. First, the exchange theory is briefly described. Second, we describe computer simulations that examine when vascular proton exchange leads to inaccuracies in the measurement of blood volume. Third, to demonstrate whether the simulated conditions are biologically relevant, we report T_1 and signal intensity measurements made in rat tumor, muscle, and liver tissue. Finally, we analyze, through simulations, methods for measuring blood volume that minimize the exchange dependence. The methods are based on the observation of Hazlewood *et al.* (13) that the initial slope of the signal enhancement curve is independent of exchange, and have been used recently to measure blood volume in liver (14). The goal of these last simulations is to provide a more comprehensive, working understanding of the accuracy and precision of blood volume measurements made from these exchange-minimization methods, and the trade-offs that the experimentally controllable parameters allow for these measurements.

THEORY

A simple mathematical model describing the relationship between the MR signal and proton exchange was presented by Hazlewood *et al.* (13) who applied a two-site exchange model to a biophysical system. Although this model can be used to describe exchange between

MRM 36:858–867 (1996)

From the Department of Radiology, Massachusetts General Hospital, MGH-NMR Center, and Harvard Medical School, Boston, Massachusetts.

Address correspondence to: Kathleen M. Donahue, Ph.D., Biophysics Research Institute, Medical College of Wisconsin, 8701 Watertown Plank Road, Milwaukee, WI 53226.

Received December 29, 1995; revised May 28, 1996; accepted May 28, 1996.

This work was supported by NIH Grants HL39810 and CA66072.

0740-3194/96 $3.00

multiple compartments, for our purposes of evaluating the MR measurement of blood volume with an intravascular T_1 contrast agent, we will use a two-compartment (vascular-extravascular) version of the model. Thus, our focus will be on the movement of water across the capillary barrier, i.e, the vascular-extravascular proton exchange. Use of the model in this manner assumes that the movement of protons between cellular and extracellular spaces is very rapid, thus enabling us to treat the tissue cells and interstitium as one extravascular space, and the red blood cells and plasma as one vascular space. This assumption is supported by the literature (10, 15–17).

The Hazlewood model is given here for the case of T_1 decay (using an inversion recovery (IR) sequence) for all conditions of exchange between the vascular (v) and extravascular (ev) compartments:

$$S_t(t) = f_v' M_o(1 - 2\exp(-\mathrm{TI}/T_{1v}')) + f_{ev}' M_o(1 - 2\exp(-\mathrm{TI}/T_{1ev}')) \quad [1]$$

where

$$\frac{1}{T_{1v}'} = C_1 + C_2,$$

$$\frac{1}{T_{1ev}'} = C_1 - C_2,$$

$$f_v' = \frac{1}{2} - \frac{1}{4}\left[(f_{ev} - f_v)\left(\frac{1}{T_{1v}} - \frac{1}{T_{1ev}}\right) + \frac{1}{\tau_v} + \frac{1}{\tau_{ev}}\right] \Big/ C_2$$

$$f_{ev}' = 1 - f_v'$$

in which

$$C_1 = \frac{1}{2}\left[\frac{1}{T_{1v}} + \frac{1}{T_{1ev}} + \frac{1}{\tau_v} + \frac{1}{\tau_{ev}}\right]$$

$$C_2 = \frac{1}{2}\left[\left(\frac{1}{T_{1v}} - \frac{1}{T_{1ev}} + \frac{1}{\tau_v} - \frac{1}{\tau_{ev}}\right)^2 + \frac{4}{\tau_v \tau_{ev}}\right]^{1/2}$$

S_t is the tissue (i.e, the vascular plus extravascular spaces) signal intensity while M_o is the equilibrium magnetization. The variables f_v and f_{ev} represent the physiological or true fractional population of protons in the vascular and extravascular compartments having inherent relaxation times T_{1v} and T_{1ev}. (Note that in this report vascular fraction (f_v) and blood volume are synonymous; both are defined as the fraction of an MR pixel that is blood. Therefore, these terms will be used interchangeably.) The observable parameters, denoted as the primed parameters (f_v', f_{ev}' and T_{1v}', T_{1ev}') are the parameters that would result from a biexponential fit of the data. How well the observable fractions and relaxation times represent the true parameters depends on the rate of proton exchange between the compartments, $1/\tau = 1/\tau_v + 1/\tau_{ev}$, where τ_v and τ_{ev} are the average residence times of a proton in the vascular and extravascular compartments. Only when τ is infinite are the observable fractions and relaxation times exactly equal to the true fractions and relaxation times. Under this "no-exchange" condition, f_v can be exactly determined from the ratio of tissue and vascular signal intensity differences (pre and post contrast):

$$f_v = \frac{\Delta S_t}{\Delta S_v} \quad [2]$$

where ΔS_v is determined from a blood sample or an image region of interest within a vessel.

As the exchange rate increases the difference between the observable and true fractional volumes and relaxation rates increases. Consequently, in the limit where $\tau_v \to 0$, f_v' becomes negligible and Eq. [1] becomes:

$$S_t(t) = \left(1 - 2 \cdot \exp^{-t}\left(\frac{f_v}{T_{1v}} + \frac{f_{ev}}{T_{1ev}}\right)\right) \quad [3]$$

In this fast-exchange limit, the relaxation rate is independent of the exchange rate and equal to the weighted sum of the compartmental relaxation rates. In this case f_v can be determined from the ratio of the difference between precontrast and postcontrast tissue and vascular T_1 relaxation rates:

$$f_v = \Delta\frac{1}{T_{1t}} \Big/ \Delta\frac{1}{T_{1v}} \quad [4]$$

where $\Delta(1/T_1)_v$ is determined from a blood sample or an image region of interest within a vessel.

Although it is unlikely that either exchange limit ($\tau = 0,\infty$) ever applies to physiological systems, it is generally thought that if the exchange rate is at least much greater than (fast-exchange) or much less than (slow exchange) the difference between the vascular and extravascular T_1 relaxation rates (18) the "no-exchange" and "fast-exchange" models represented by Eqs. [2] and [4] may still give accurate measures of f_v. Whether this is true is addressed with the simulations and experiments presented below.

METHODS

The Methods are presented in three parts. First we describe the general exchange simulations that were used to evaluate the influence of vascular exchange on blood volume measurements. Second, details regarding the measurements made in a rat model are given. Finally, we present the details of the simulations that we performed to examine exchange-minimization methods for measuring blood volume.

General Exchange Simulations

To evaluate the implications of exchange when using the fast and no-exchange models, we modeled a more complete system. Specifically, given an f_v of 0.10, Eq. [1] was used to calculate the signal intensity at the 10 inversion times (TI = 0.05, 0.2, 0.4, 0.8, 1.2, 2.0, 3.0, 4.0, 7.0, 10.0 s). (These times are equivalent to those used in the measurements described below.) This was repeated for a range of biologically relevant exchange rates (1–10 s^{-1})

(9, 19, 20) and vascular contrast agent concentrations ($\Delta R1 = 0.0–10.0\ s^{-1}$). Then, either the no-exchange (Eq. [2]) or fast-exchange (Eq. [4]) model was used to calculate f_v. For the fast-exchange model, where T_1 decay is assumed monoexponential, a Simplex fitting algorithm (21) was used to fit the data to the three-parameter T_1 decay equation:

$$S_{tot} = M_o(1 - 2\ a\ \exp^{(-TI/T_{1o})}) \quad [5]$$

where M_o is the equilibrium magnetization and a is the factor used to compensate for imperfect inversion. (For the simulations $a = 1.0$.) Because of the short TE used in the experiments (2.5 ms), we ignored the T_2 contribution to this equation. When using the no-exchange model, f_v was determined from the difference between postcontrast and precontrast signal intensities at TI = 0.8 s, the TI that is used for maximum contrast (i.e, where $TI \approx T_1$).

Measurements

Ten female Fischer 344 rats weighing approximately 150 g were implanted with the R3230 mammary adenocarcinoma harvested from flank tumor fragments of donor rats. Measurements were made approximately 14 days after implantation. Following the MR imaging procedure, the animals were euthanized by pentobarbital overdose (120 mg/kg intravascularly).

All studies were performed on a 2T SISCO NMR imaging spectrometer (Varian Associates, Inc., and Spectroscopy Imaging Systems Corporation, Fremont, CA). The MR experiment entailed injecting five to six doses (14 μmole Gd/kg each) of a novel, long-lived contrast agent (blood half life ~14 h), MPEG-PL-Gd-DTPA (22). (The calculated molecular weight of MPEG-PL-Gd-DTPA is 560 kD on the basis of elemental analysis. It has an apparent hydrodynamic diameter of 1160 kD protein by HPLC due to the brush effect where polymer chains of MPEG stick out and make it look heavier than it actually is. Its T_1 relaxivity in saline is 11.4 s^{-1} per mM of Gd^{3+} at 2.0 T and 36°C.) After each injection images were acquired at 10 inversion times (0.05, 0.2, 0.4, 0.8, 1.2, 2.0, 3.0, 4.0, 7.0, 10.0) using an IR turbo-FLASH sequence (TE = 2.5 ms, TR = 7 ms, flip = 11°, image matrix: 64 × 64) segmented into four acquisitions to minimize T_1 decay during each acquisition. The intersegment delay was 7 s to allow for full T_1 relaxation between acquisitions. (To validate the T_1 measurement accuracy of this sequence, turbo-FLASH measured T_1s were compared with spectroscopically measured T_1s of phantoms whose T_1 values ranged from 200 to 800 ms. With the total acquisition segmented into four acquisitions, the turbo-FLASH measured T_1s were within 3% of the spectroscopically measured T_1s.) Following the last injection, T_1 was measured approximately every 5 min over a 30- to 70-min period to assess the possibility of extravascular leakage of the agent. A standard IR spectroscopy sequence was used to measure the blood T_1s sampled before and immediately after the imaging experiment. Assuming that the intravascular contrast agent builds linearly with injection (because of the long clearance time), the blood relaxation rates for each dose were computed from preexperiment and postexperiment blood T_1s. Subsequently f_v was determined using either the fast or no-exchange model as described above. To evaluate the no-exchange model the difference in precontrast and postcontrast signal intensities was determined at TI = 0.8 s.

The data were summarized by determining the mean f_v from all rats and the standard error of the mean (SE), for both the no-exchange and fast-exchange models. Since there was some variation in the blood $\Delta R1_v$ values for each rat, a curve was fit to the data from each rat using a locally weighted least squared error method. Subsequently, the f_v values at $\Delta R1$ = 2.0, 4.0, 6.0, and 8.0 s^{-1} were determined from the fitted curves and used to calculate the mean f_v and SE.

Exchange-Minimization Simulations

The initial slope of the relaxation curve (Eq. [1]) with TI is independent of the exchange rate (13), and thus, to first order in TI, signal changes for small TI do not depend on exchange. Therefore, for short enough TI, both the fast and no-exchange models do not depend on exchange, and should give the same results. We test this concept in the simulations presented here. We evaluate both Eqs. [2] and [4] using an IR sequence, and extend the methodology to non-IR imaging by evaluating the no-exchange model when using a simple transverse-spoiled gradient echo sequence (GRE). Throughout the remainder of this report, these methods will be referred to as exchange-minimization (EM) methods.

For an IR sequence, the fast and no-exchange models give equivalent estimates of blood volume, and are therefore minimally sensitive to exchange when $TI \ll T_{1v}', T_{1ev}'$. Therefore, either the signal intensity can be measured at a given TI and the no-exchange model (Eq. [2]) used to determine f_v or, T_1 can be determined from signal intensities measured at several TI values (all $\ll T_{1v}', T_{1ev}'$) and the fast-exchange model (Eq. [4]) used to determine f_v. We will refer to these methods as "no-exchange, exchange-minimized IR" (nEM-IR) and "fast-exchange, exchange-minimized IR" (fEM-IR) methods.

An alternative exchange-minimization approach is to use a transverse-spoiled gradient echo (GRE) pulse sequence with very short TRs. For the fast and no-exchange models to give equivalent blood volume estimates (and therefore be minimally sensitive to vascular exchange), the conditions that $TR \ll T_{1v}', T_{1ev}'$ and

$$\frac{\cos\alpha}{1-\cos\alpha}\frac{TR}{T_1} \ll 1 \quad [6]$$

must be satisfied, where α denotes the flip angle, and T_1 represents the postcontrast T_{1v}' or T_{1ev}'. Although Eq. [6] was derived from the limiting cases of exchange (see the derivation in the Appendix), since the signal intensity is a monoexponentially increasing function of exchange rate (23), this condition will hold for all exchange conditions. With this method f_v is determined from GRE signal intensity differences, i.e, by using the no-exchange model described by Eq. [2]. This method will be referred to as "no-exchange, exchange-minimized GRE" (nEM-GRE).

To evaluate the accuracy and precision of the exchange-minimization methods, the general exchange

simulations described above were repeated with slight modifications. For the case where the fEM-IR method was used, signal intensities were determined at TI values much shorter than (TI $\ll T_{1v}$: 0.04, 0.07, 0.1 s) the postcontrast vascular T_1 relaxation time (0.5 s). An apparent T_1 was then determined by fitting these signal intensities and the signal intensity determined at one longer value (TI = 5.0 s; for estimation of M_o) to Eq. [5]. The tissue T_1 was calculated in this way for both the precontrast and postcontrast conditions where the precontrast vascular T_1 was assumed equal to 1.0 s. From these T_1 measurements f_v was computed using Eq. [4]. Similarly, for the nEM-IR method, f_v was computed using the no-exchange model (Eq. [2]) at a TI value of 0.1 s. This TI value was chosen because it is the value from the TI list used for the fEM-IR simulations, where the greatest difference in precontrast and postcontrast signal intensities will occur. Finally, the no-exchange model was used to compute f_v for the case where a transverse-spoiled GRE sequence was used. Specifically, f_v was calculated as a function of exchange rate for *TR* values of 10, 50, and 100 ms for flip angles ranging from 10°-90°.

Although exchange-minimization methods may provide more accurate measures of blood volume, measurement precision may suffer since minimizing the effect of exchange usually comes by imaging at TI or *TR*/flip combinations that do not maximize contrast-to-noise. Therefore, to evaluate both accuracy and precision of these exchange-minimization methods, we added experimental noise to the simulations just described. To appropriately model the noise in the MR signal, the signal magnitude with noise was set equal to:

$$\sqrt{\left[\left(M+\frac{n_1}{\mathrm{SNR}}\right)^2+\frac{n_2^2}{\mathrm{SNR}}\right]} \qquad [7]$$

where M is the signal magnitude without noise, normalized to $M_o = 1.0$, and $n_{1,2}$ are the random numbers drawn from a Gaussian distribution with zero mean and unit variance (21). For a given set of conditions, as described above, 10^4 iterations were performed from which a mean f_v was determined along with its standard deviation. To compare the fEM-IR, nEM-IR, and nEM-GRE methods, a 5-min experiment was simulated where the SNR of the fully relaxed signal (M_o) was assumed to be 100. For the fEM-IR method, with a *TR* of 6.0 s, 12 averages can be acquired at each TI value (assuming a small total acquisition time (e.g., ≈ 30 ms) as would be true when using an IR echo planar sequence) increasing the effective signal-to-noise ratio (SNR) per TI value to approximately 350. For the nEM-IR experiment, in 5 min, 48 averages can be acquired at one TI value giving an effective SNR of about 700. For the nEM-GRE experiment, simulations were performed for *TR* values of 10, 50, and 100 ms. For each nEM-GRE experiment, where use of a conventional (non-EPI) pulse sequence is assumed, the SNR used in Eq. [7] was set to reflect the chosen *TR*. For example, with a *TR* of 10 ms and 64 phase encoding steps, approximately 470 averages can be acquired in 5 min. Also, with *TR* = 10 ms, the total acquisition time is reduced by approximately ⅓ relative to the IR-EPI experiments where a typical acquisition time is 30 ms. Since the SNR is directly proportional to the square root of the number of averages and the square root of the acquisition time, the SNR that would be used in Eq. [7] is equal to $100 \cdot \sqrt{470} \cdot \sqrt{10/30} \approx 1252$.

In summary, assuming a true $f_v = 0.10$, we estimated a mean and standard deviation of the measurement for each of the exchange-minimization methods using a fixed, 5-min total measurement time. The simulations were performed for vascular exchange rates ranging from 1.0 to 31 s^{-1}, and T_{1v}s of 500, 200, and 100 ms.

RESULTS

General Exchange Simulations

Figure 1 illustrates the effect of vascular proton exchange when using either a no-exchange or fast-exchange model to determine f_v. The upper three curves represent the case where the no-exchange model was used. The calculated f_v provides a fairly accurate measure of f_v (0.1) for very low contrast concentrations, but then proceeds to overestimate the blood volume as the concentration increases. As the vascular exchange rate is increased, the overestimation worsens. Note that because of finite exchange, even when the slow exchange condition is satisfied ($1/\tau \ll \Delta R1_v$), the measured f_v will overestimate the true f_v. For example, with $1/\tau = 1\ s^{-1}$, which is much less than $\Delta R1_v = 10\ s^{-1}$, the f_v is overestimated by almost 20%. The lower three curves in Fig. 1 represent the case where the fast-exchange model was used to calculate f_v. The measurement is quite accurate at low concentrations, but underestimates the true f_v at higher concentrations. The underestimation worsens with a decrease in the vascular proton exchange rate.

Measurements

The summarized blood volume measurement results from tumor, muscle, and liver tissue are given in Fig. 2.

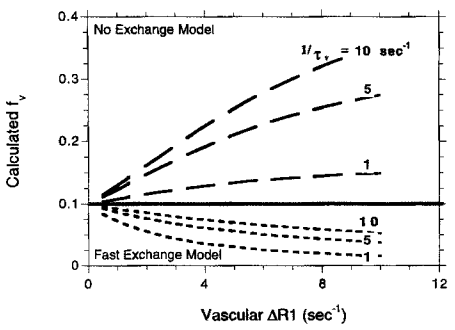

FIG. 1. Computer simulation results demonstrating the influence of the vascular proton exchange rate ($1/\tau_v$) on the measurement of f_v. The top three curves represent the f_v calculated when using the no-exchange IR model at TI = 0.8 s. Under this condition, the calculated f_v may significantly overestimate the true f_v (= 0.10, represented by the solid line). The overestimation worsens with an increase in vascular contrast concentration and $1/\tau_v$. The lower three curves represent the f_v calculated from the fast-exchange model when using an IR sequence with a TI list which samples the entire T_1 decay curve (TI = 0.05, 0.2, 0.4, 0.8, 1.2, 2.0, 3.0, 4.0, 7.0, 10.0 s). Under these conditions, the true f_v can be significantly underestimated. The underestimation increases with contrast concentration and a decrease in $1/\tau_v$.

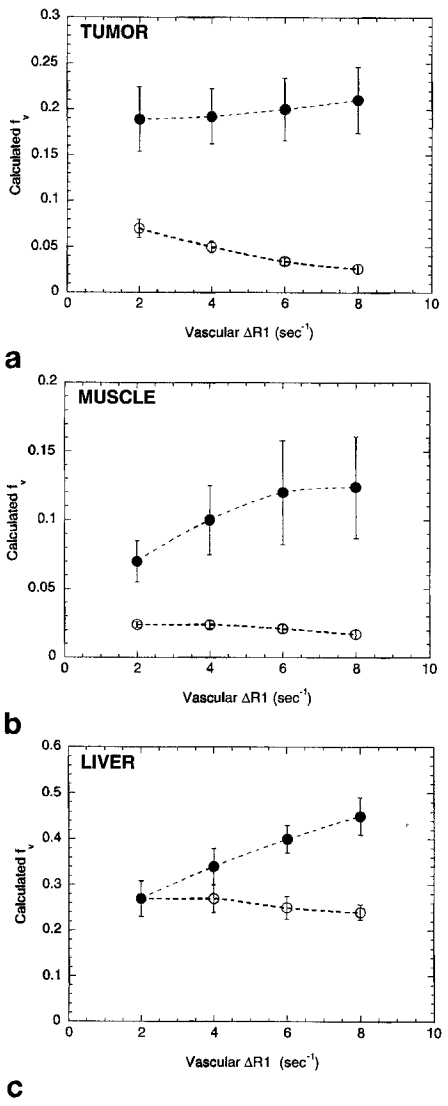

FIG. 2. Mean and standard error of f_v measurement results from tumor (a), muscle (b), and liver (c) tissue when using the no-exchange (filled circles) and fast-exchange (open circles) methods. Since there was some variation in the blood $\Delta R1_v$ values for each rat, a curve was fit to the data from each rat using a locally weighted least squared error method. Subsequently, the f_v values at $\Delta R1 = 2.0, 4.0, 6.0$, and $8.0\ s^{-1}$ were determined from the fitted curves and used to calculate the mean f_v and SE values shown here.

The averaged tumor and muscle data are for six rats, while the liver data are shown for four rats. Results from all 10 rats were not included since rat #8 did not survive the MR experiment and data in rat #9 were not acquired at $\Delta R1_v$ less than $5\ s^{-1}$. In addition, in some cases the delayed images showed continued extravascular leakage of the agent (rat #2: muscle, rat #3, 5: tumor, rat #7: liver) making the result indeterminable. Finally, the muscle f_v for rat #10 was not discernable due to inadequate SNR on that experiment day, and liver tissue was not in the imaging slice for three of the nine (surviving) cases.

For the remaining four to six rats, the experimental results demonstrate trends similar to those predicted by the simulation results shown in Fig. 1. In particular, when the no-exchange model was used with TI = 0.85 s (filled circles), the f_v calculated in both muscle and liver tissue increased with vascular contrast concentration, comparable with the upper curves of Fig. 1. While a similar trend is less apparent in the averaged tumor data, it becomes more apparent when viewing the tumor data on an individual basis, examples of which are given in Fig. 3. (The fact that the averaged tumor data masks individual trends is most likely a result of the greater variability in blood volume and vascular permeability parameters typical of tumors.) When the fast-exchange model (open circles) was used, the calculated tumor f_v decreased with contrast concentration, comparable with the lower curves of Fig. 1. While some decrease in f_v with concentration is apparent in both muscle and liver tissue, the decrease is much less pronounced.

A summary of all results (including those from rat #9) can be found in Table 1, which lists the calculated f_v results determined at high contrast concentrations ($\Delta R1 \approx 6-8\ s^{-1}$); (to the right of the representative curves shown in Fig. 2).

Exchange-Minimization Simulations

The simulation results in Figs. 4-7 explore the accuracy and precision of exchange-independent methods. When the blood is doped to a T_1 of 500 ms, using the fEM-IR method, the mean values are within 5% of the true value but have standard deviations of as much as 50% (Fig. 4a). As demonstrated in Fig. 4b, when using the nEM-IR method at TI = 0.1s, the apparent f_v is within 2% of the true f_v while the standard deviation remains less than 10%, that is, both the accuracy and the precision have been improved. With a higher vascular contrast agent concentration, yielding a blood T_1 of 200 ms (Figs. 4c and 4d), the measurement precision improves but the accuracy worsens since the exchange-minimization conditions are less well satisfied. Similarly, if longer TI values are used, the precision will improve while the accuracy worsens.

The nEM-GRE simulation results are given in Figs. 5 and 6. Figure 5 shows the calculated f_v and standard deviation of this calculation for a range of *TR* values and as a function of flip angle for a vascular exchange rate of $31\ s^{-1}$. The $31\ s^{-1}$ exchange rate was chosen as it gives the worst case scenario for the range of exchange rates evaluated in this report. While a 90° flip angle with short *TR* appears best for the most accurate measure of f_v (Fig. 5a), a finding consistent with Eq. [6], a flip angle of about 30°-50° and short *TR* appears to be the most precise (Fig. 5b). Calculated f_v as a function of exchange rate is shown in Fig. 6 for a *TR* of 10 ms and flip angles of 30° and 50°.

DISCUSSION

The exchange simulations and measurements presented here demonstrate the importance of considering vascular proton exchange when using intravascular T_1 contrast agents to measure blood volume fraction. The general exchange simulations demonstrated that when using either the no or fast-exchange models, the true vascular volume can be substantially overestimated or underestimated, respectively. The magnitude of the inaccuracy

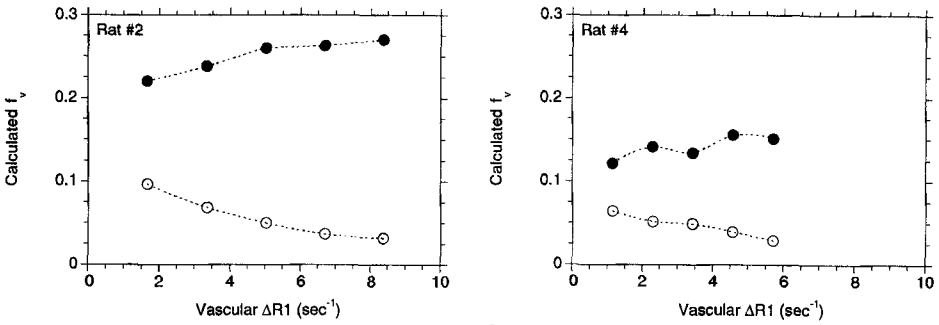

FIG. 3. Representative f_v measurement results from the tumor tissue of rat #2 (a) and rat #4 (b). The filled circles represent the f_v calculated when using an IR sequence and the zero exchange model for TI = 0.8 s. The open circles represent the f_v calculated when using the IR sequence and the fast-exchange model for a TI list that samples the entire T_1 decay curve (TI = 0.05, 0.2, 0.4, 0.8, 1.2, 2.0, 3.0, 4.0, 7.0, 10.0 s). Typically, as demonstrated here, the individual tumor results demonstrate that the calculated f_v increases with concentration when using the no-exchange method and decreases with concentration when using the fast-exchange calculation method.

depends on both the exchange rate and experimental parameters. T_1 and signal intensity measurements made in the rat model demonstrate that these theoretical findings are biologically relevant, and that simple exchange models may result in f_v measurements that are strongly dependent on the experimental parameters. As can be seen from Table 1, with well-doped blood, the estimated vascular volume fractions for tumor and muscle differ by roughly a factor of 5 depending on the exchange assumptions.

The general behavior of blood volume estimates in the exchange simulations can be explained by their limits. The no-exchange simulation results (Fig. 1, upper curves) may initially seem surprising; it seems that when using the no-exchange model, the measurement accuracy should improve as the slow exchange condition ($1/\tau \ll R1_v - R1_{ev}$, where $1/\tau = 1/\tau_v + 1/\tau_{ev}$) is better satisfied, that is, as $R1_v$ is increased. However, for a given exchange rate, the overestimation of blood volume actually worsens with an increase in contrast concentration. This result can be explained by the fact that even under slow exchange conditions, the observed relaxation rates still depend on exchange:

$$R1_{ev}(\text{high concentration}) = R1_{ev}(\text{pre-contrast}) + \frac{f_v(\text{true})}{\tau} \quad [8]$$

$$R1_v(\text{high concentration}) \approx R1_{v(\text{pre})} + \Delta R1_v + \frac{1 - f_v(\text{true})}{\tau} \quad [9]$$

So, for example, when the T_1 of the blood is made very short so that $R1_v \gg R1_{ev}$, ($R1_v \gg 1/\tau$), it does not mean that the second term in Eq. [8] can be neglected. Thus, even in "slow" exchange, significant exchange can modify the signal, shortening the apparent T_1 of the "extravascular" compartment. As a result, under slow exchange conditions, and assuming the blood compartment is completely relaxed, the calculated f_v approaches a value that is dependent on the exchange rate and TI:

$$f_v(\text{calculated, slow}) = f_v(\text{true})\left(1 + \frac{\text{TI}}{\tau}\right) \quad [10]$$

Thus, a longer TI allows more time for extravascular spins to enter the vascular space, and be affected by the contrast agent, a condition that appears as a larger apparent vascular space.

The shape of the fast-exchange model estimates (Fig. 1, lower curves) also depends on the correctness of the exchange assumption. Since fast-exchange is defined as the condition where the exchange rate is much greater than the difference between the vascular and extravascular T_1 relaxation rates ($1/\tau_v \gg R1_v - R1_{ev}$) (18), at the lowest contrast concentrations the fast-exchange condition is satisfied (since $R1_v \approx R1_{ev}$), and the measurement of vascular fraction should be accurate. As the contrast concentration increases or the exchange rate decreases, the fast-exchange condition is less well satisfied and the measurement becomes increasingly inaccurate. In the high contrast concentration limit where the exchange is slow ($1/\tau_v \ll R1_v - R1_{ev}$) and fast-exchange is assumed (monoexponential T_1 decay), using Eqs. [8] and [9], the calculated f_v approaches the following limit:

$$f_v(\text{calculated, fast}) = f_v(\text{true})\frac{(1 + \text{TI}\ 1/\tau)}{\text{TI}\ R1_v} \quad [11]$$

Consistent with the simulation results of Fig. 1, the underestimation of f_v(true) increases with concentration. In the high concentration limit, by taking the ratio of Eqs. [10] and [11], we see that the f_v(calculated slow)/f_v(calculated fast) $\approx$ TI R_v, which is consistent with the data given in Table 1 for tumor and muscle. For liver, the contrast concentrations were not high enough to reach this limit.

In summary, with a finite exchange of protons, measurement accuracy will depend on both the exchange

Table 1
Measurement Summary

Tissue	Calculated f_v ($\Delta R1_v \approx$ 6–8 s^{-1})	
	No-exchange model	Fast-exchange model
Tumor	0.19 ± 0.07 (n = 7)	0.029 ± 0.01 (n = 7)
Muscle	0.08 ± 0.03 (n = 7)	0.015 ± 0.01 (n = 7)
Liver	0.41 ± 0.06 (n = 5)	0.26 ± 0.07 (n = 5)

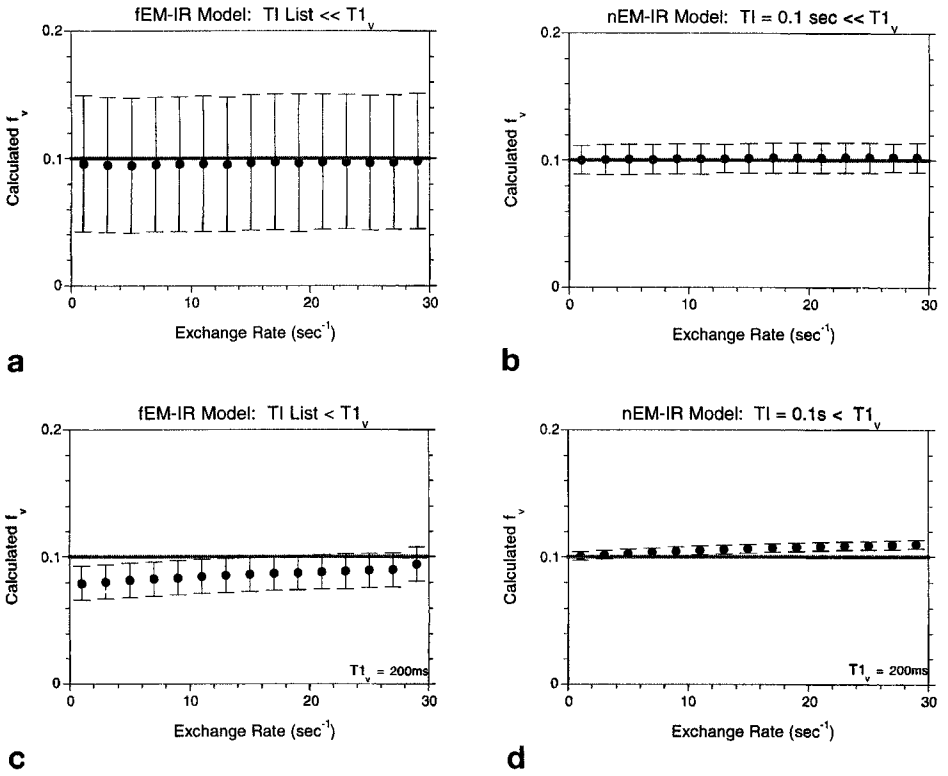

FIG. 4. Accuracy and precision of IR exchange independent methods. (a) When the initial slope is measured and the fast-exchange model used to calculate f_v (fEM-IR method), the accuracy (mean f_v) is within 5% of the true value (0.1) while the precision (standard deviation) is near 50%. (b) When the initial slope is measured and the no-exchange model (nEM-IR) is used to calculate f_v, the accuracy is with 2% of the true f_v, while the standard deviation remains less than 10%. Increasing the contrast concentration (T_{1v} = 200 ms), results in an increased accuracy and decreased precision for both the (c) fEM-IR and (d) nEM-IR methods.

rate and measurement parameters, with measurement accuracy improving as TI decreases.

The rat measurement results are consistent with the general exchange simulation results: the f_v will be underestimated if fast-exchange is assumed, and it isn't; or overestimated if no-exchange is assumed, and exchange is present. Although neither the vascular exchange rate nor blood volume fraction were independently known, the trends in f_v with concentration are consistent with exchange rates that are finite but not decidedly fast relative to the apparent compartmental relaxation rates. In particular, for tumor neither the fast nor no-exchange models appeared appropriate (they were concentration-dependent) for the measure of f_v, a finding suggestive of tumor vascular exchange that is intermediate. For muscle and liver tissue the calculated f_v was strongly dependent on concentration with the simplified no-exchange model, but much less sensitive to contrast concentration when using the fast-exchange model. Despite this result, one must be cautious in the decision to use the simplified fast-exchange model for blood volume measurements in these tissues. First, the fast-exchange model appears accurate simply because its results are being compared with the no-exchange results which are quite concentration-dependent for the TI value used. (One may arrive at the opposite conclusion if the fast-exchange results were compared with no-exchange results derived at shorter TI values.) Furthermore, when using the simplified fast-exchange model, the mean muscle f_v at $\Delta R1_v = 8\ s^{-1}$ is 30% less than the mean f_v at $\Delta R1v = 2\ s^{-1}$, a decrease that may not be acceptable. However, for liver the decrease in f_v between $\Delta R1_v = 2s^{-1}$ and $8\ s^{-1}$ is only 12%

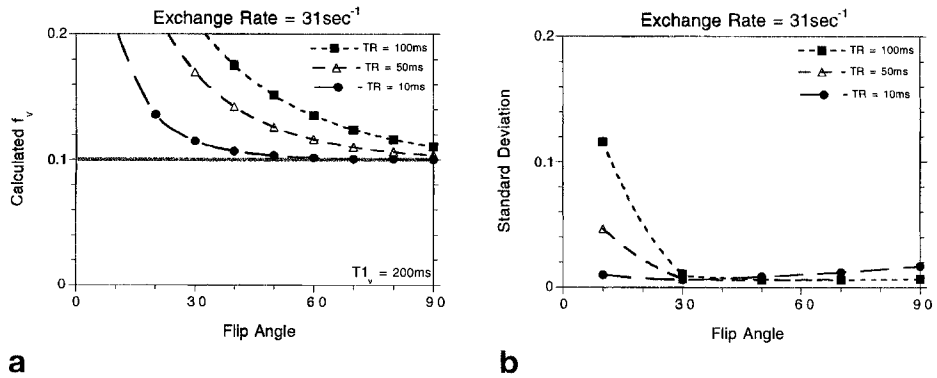

FIG. 5. The accuracy and precision of the no-exchange, GRE method (nEM-GRE), assuming an f_v of 0.10, T_{1v} = 200 ms, and a vascular exchange rate of 31 s^{-1}. (a) The calculated f_v as a function of flip angle for *TR* values of 10, 50, and 100 ms. The accuracy improves with an increasing flip angle and decreasing *TR*. (b) The standard deviation of the f_v measurement as a function of flip angle and *TR*. The best precision (lowest standard deviation) results when the flip angle is approximately 30°-50°.

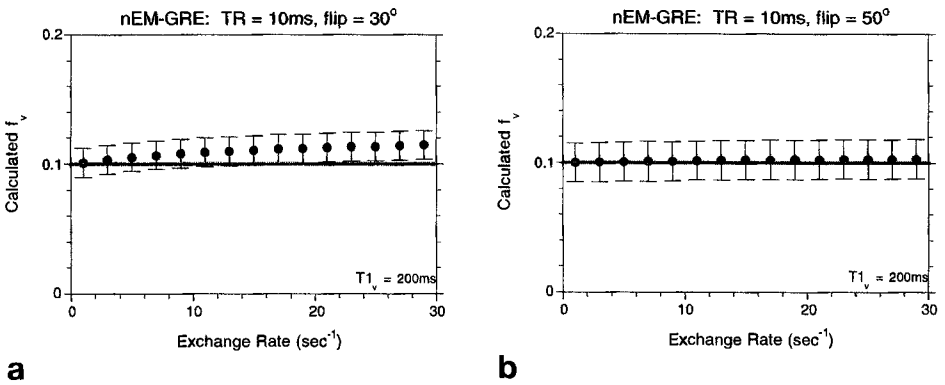

FIG. 6. Calculated f_v as a function of exchange rate for a *TR* of 10 ms and a flip angle of (a) 30° and (b) 50°.

suggesting that this model may give sufficiently accurate measurements of liver f_v, at least for the experimental conditions used here. Whether the simplified fast-exchange model would in fact provide accurate measures of liver blood volume, and under what conditions, requires additional studies that include independent correlative measures of either the vascular blood volume or exchange rate.

Of the exchange-minimization methods evaluated, methods that used the no-exchange model to calculate f_v (nEM-IR, nEM-GRE) proved to be the most feasible giving both very good accuracy and better precision than the fast-exchange IR model (fEM-IR). The better precision of the no-exchange models is not due to the underlying exchange assumption of the model. Rather, these models proved most precise simply because the measurement was derived from the signal intensity on the initial slope instead of measuring the initial slope itself. As a result, all of the imaging time could be spent at the inversion time that was more sensitive to signal differences. In general, the nEM-IR and nEM-GRE may also be easier to implement than the fEM-IR method. The nEM-IR method does not require inversion times as short as those needed for the fEM-IR method and short *TR* sequences are readily available on most MR imaging systems. Furthermore, with the nEM-GRE method the capability of using very short *TR*s enables use of higher contrast concentrations with the initial slope condition still easily satisfied. Finally, when using a transverse-spoiled GRE sequence to measure blood volume the measurement accuracy and precision can be maintained for a variety of flip angle/*TR* combinations.

To summarize the trade-offs and dependencies of the GRE method, and to give some guidance in the choice of imaging parameters, we generated the graphs shown in Fig. 7. Figure 7a depicts flip angle as a function of accuracy for *TR* values ranging from 10 to 100 ms, with T_{1v} = 200 ms and f_v = 0.10. Since the accuracy (how close the mean value is to the true value) is primarily a function of the correctness of the exchange assumptions, the measurement accuracy in this graph was defined as the ratio of the blood volume, determined from the no-exchange model, to that determined when using the fast-exchange model. When this ratio is equal to 1.0, the measurement is exchange independent, and the best accuracy is achieved. From this figure it is apparent that for a desired accuracy, a multitude of flip angle/*TR* combinations can be chosen. However, note that as the *TR* increases, the maximum achievable accuracy decreases.

Another factor that must be considered when choosing a flip angle/*TR* combination is measurement precision. Figure 7b depicts measurement precision as a function of accuracy, which is defined the same as in Fig. 7a. In this figure measurement precision, which is proportional to the SNR of the blood volume estimate, was estimated from $\Delta M/\sqrt{TR}$, where ΔM is the signal difference that would result for a given flip angle, *TR*, and blood volume. The solid curve represents the case where T_{1v} = 100 ms and *TR* = 10 ms, while the dashed curve represents the case where T_{1v} = 200 ms and *TR* = 10 ms. For each curve the flip angle increases from left to right, from 0° to 90°. Therefore, each point on these curves represents the accuracy and precision that would result for a certain flip angle with *TR* = 10 ms. Performing an experiment with values that lie to the left of the curve maxima would not be optimal since both accuracy and precision can be improved by choosing values further to the right, i.e, by increasing the flip angle when *TR* is fixed. A useful trade-off between accuracy and precision occurs for flip angle/*TR* combinations that occur at the peak of the curves and to the right. In these regions, increasing the flip angle, with a fixed *TR*, may result in improved accuracy but less precision. Somewhat surprisingly, for a given T_{1v}, the curves shown in Fig. 7b are almost exactly the same regardless of the *TR* chosen. That is, while the specific flip angle that corresponds to a given measurement accuracy does depend on *TR* (Fig. 7a), once that accuracy is specified, the precision evaluated at that flip angle is independent of *TR*. For example, when T_{1v} = 100 ms, an accuracy and precision of approximately 0.6 and 0.19 can be achieved with a multitude of *TR*/flip angle combinations two of which are 10 ms/19° and 100 ms/55°. Consequently, since the desired precision can be achieved at almost any *TR* value we say that the precision is independent of *TR*. The one exception is that the extent of the curve to the far right in Fig. 7b does depend on *TR*: the curves can have *x* axis points closer to 1 at shorter *TR*s. For example, for a flip angle of 90°, when *TR* = 10 ms the precision/accuracy value will be further to the right (more accurate and less precise) than when *TR* = 50 ms. In other words, the precision/accuracy that can be achieved with *TR* = 10 ms/flip = 90° cannot be achieved when *TR* = 50 ms.

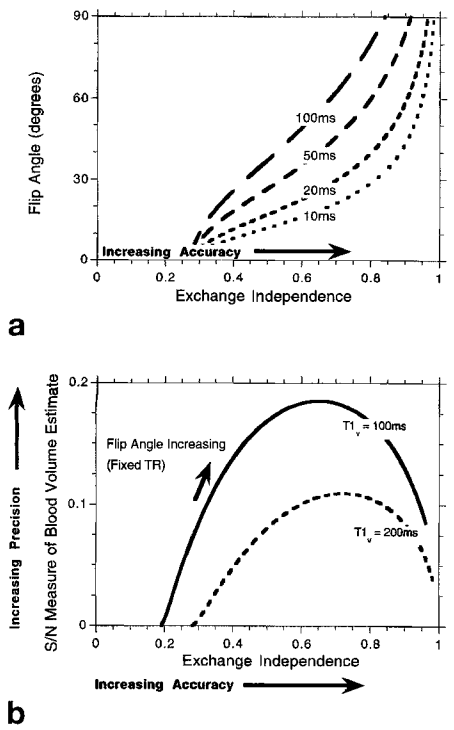

FIG. 7. Summary of the accuracy/precision trade-offs of the GRE method. (a) Flip angle as a function of accuracy for *TR* values of 10, 20, 50, and 100 ms. (b) Precision as a function of accuracy for a *TR* of 10 ms and T_{1v} = 100 ms (solid line) and for *TR* = 10 ms and T_{1v} = 200 ms (dashed line). The flip angle increases from left to right 0°-90°.

To simplify the comparison of precisions, we assumed that the actual encoding times per slice (i.e., bandwidth) was the same for all techniques. As a result, precision estimates at the longer *TR* may underestimate their relative performance if the bandwidth were narrowed as the imaging time increased.

The exchange minimization results are concordant with those of Schwickert *et al.* (14) who used exchange-minimization methods to measure liver blood volume. Specifically, they found that liver blood volume could be accurately determined from ΔR1 (using the fast-exchange model), and either an ultrashort TI IR sequence or a 3D-SPGR sequence (3D spoiled gradient recalled acquisition in a steady state). The model choice was reasonable given the measurement results presented here, which indicate that the simplified fast-exchange model may be appropriate for the measurement of liver blood volume fraction. In other tissues where the simplified exchange models are not appropriate, this technique should yield additional improvements in the accuracy of the blood volume measurement.

An alternate method for measuring blood volume, which also takes vascular exchange into account, would be to fit the data for blood volume and exchange rate using general exchange equations such as those given by Eq. [1]. However, our experience with using multiparameter, nonlinear fits of the imaging data was that the resulting fits showed very large covariance between the fitted parameters: that is, trade-offs between blood volume and exchange fit the data equally well. However, with the appropriate pulse sequence and sufficient SNR, a full fit for blood volume and exchange may prove to be a feasible approach.

In view of the recent developments of high speed computed tomography (CT), one may wonder whether CT, which is not sensitive to water exchange, would be better for the measurement of total blood volume. However, as demonstrated in this report, with the effect of exchange well understood, blood volume can be accurately measured with MRI methods. In addition, the MR sensitivity to water exchange can be used to our advantage. For example, it seems reasonable that the interplay between exchange and measurement parameters can be exploited to design a paradigm in which exchanging and nonexchanging vessels can be distinguished. This may prove important for issues such as drug delivery or for understanding the contribution of various-sized vessels to functional brain activation.

In summary, we have described the influence of vascular proton exchange on the measurement of blood volume, when using long-lived intravascular T_1 contrast agents. Because of intravascular/extravascular water exchange, experimental parameters must be carefully chosen to achieve the desired accuracy and precision. We have described techniques that reduce the effects of this exchange. While completely exchange-free measurements can only be made in theory, by sacrificing some accuracy, large improvements in precision of these techniques should result. Although exchange makes the analysis of blood volume measurements more complex, it may also give MRI the unique potential of deriving important information about tissue vasculature: an impetus for future studies.

APPENDIX

As stated in the METHODS section of this manuscript, when using a short-*TR*, transverse-spoiled GRE method, the measurement of blood volume fraction (f_v) from signal intensity differences (ΔS), will be minimally dependent on vascular proton exchange if $TR \ll T_{1v}', T_{1ev}'$ and the following condition is satisfied:

$$\frac{\cos\alpha}{1-\cos\alpha}\frac{TR}{T_1} \ll 1 \qquad [A1]$$

where T_1 represents either the postcontrast T_{1v}' or T_{1ev}'. (See the derivation below for clarification of this point.) This appendix demonstrates that these conditions result in a measurement that is exchange independent.

When using a short-*TR* method, the steady-state magnetization (M_{ss}) is equal to the following:

$$M_{ss} = M_o \frac{(1-\exp^{(-TR/T_1)})}{1-\cos(\alpha)\exp^{(-TR/T_1)}} \qquad [A2]$$

If $TR \ll T_1$:

$$M_{ss} = M_o \frac{TR/T_1}{1-\cos(\alpha)(1-TR/T_1)} \qquad [A3]$$

which can be rewritten as follows:

$$M_{ss} = M_o \frac{TR/T_1}{(1 - \cos(\alpha)) + \cos(\alpha)\dfrac{TR}{T_1}} \quad [A4]$$

or

$$M_{ss} = M_o - \frac{TR/T_1}{(1 - \cos(\alpha))\left(1 + \dfrac{\cos(\alpha)}{1 - \cos(\alpha)}\dfrac{TR}{T_1}\right)} \quad [A5]$$

Consequently, with the requirement that $\dfrac{\cos(\alpha)}{1 - \cos(\alpha)}\dfrac{TR}{T_1} \ll 1$:

$$M_{ss} = \frac{M_o}{1 - \cos(\alpha)} TR\,\mathrm{R1} \quad [A6]$$

where $\mathrm{R1} = 1/T_1$. Therefore, for the case of no exchange, where $T_{1v} = T_{1v}'$ and $T_{1ev} = T_{1ev}'$, the tissue signal is:

$$S_{tissue} = f_v M_o' TR\,\mathrm{R1}_v + f_{ev} M_o' TR\,\mathrm{R1}_{ev} \quad [A7]$$

where $M_o' = M_o/1\text{-}\cos(\alpha)\,(\sin(\alpha))$ and the difference between the postcontrast and precontrast signal intensities is:

$$\Delta S_{tissue} = f_v M_o' TR\,\Delta\mathrm{R1}_v \quad [A8]$$

Similarly, with fast-exchange:

$$S_{tissue} = M_o' TR\,\mathrm{R1}_{tissue} \quad [A9]$$

where $\mathrm{R1}_{tissue} = f_v\,\mathrm{R1}_v + f_{ev}\,\mathrm{R1}_{ev}$. Therefore, the difference between the postcontrast and precontrast signal intensities is:

$$\Delta S_{tissue} = M_o' TR\, f_v\,\Delta\mathrm{R1}_v \quad [A10]$$

Equations A8 and A10 are equivalent demonstrating that, under the conditions listed above, f_v can be accurately determined from ΔS_{tissue} irrespective of whether the exchange is zero or fast. When this is the case, the determination of f_v from ΔS_{tissue} is exchange-independent. Also, since the signal intensity is a monoexponentially increasing function of the exchange rate (23), under the conditions listed above, this approach will be exchange independent for all exchange conditions.

REFERENCES

1. J. W. Belliveau, D. N. Kennedy, R. C. McKinstry, B. R. Buchbinder, R. M. Weisskoff, M. S. Cohen, J. M. Vevea, T. J. Brady, B. R. Rosen, Functional mapping of the human visual cortex by magnetic resonance imaging. *Science* **254,** 716–719 (1991).
2. U. Schmiedl, M. E. Moseley, R. Sievers, M. D. Ogan, W. M. Chew, H. Engeseth, W. Finkbeiner, M. J. Lipton, R. C. Brasch, Magnetic resonance imaging of myocardial infarction using albumin-(Gd-DTPA), a macromolecular blood-volume contrast agent in a rat model. *Invest. Radiology* **22,** 713–721 (1987).
3. V. S. Vexler, Y. Berthezene, O. Clement, A. Muhler, W. Rosenau, M. E. Moseley, R. C. Brasch, Detection of zonal renal ischemia with contrast-enhanced MR imaging with a macromolecular blood pool contrast agent. *J. Magn. Reson. Imaging* **2,** 311–319 (1992).
4. J. Folkman, How is blood vessel growth regulated in normal and neoplastic tissue? *Cancer Res.* **46,** 467–473 (1986).
5. C. Schwarzbauer, J. Syha, A. Haase, Quantification of regional blood volumes by rapid T_1 mapping. *Magn. Reson. Med.* **29,** 709–712 (1993).
6. D. M. Shames, R. Kuwatsuru, B. Vexler, A. Muhler, R. C. Brasch, Measurement of capillary permeability to macromolecules by dynamic magnetic resonance imaging: a quantitative noninvasive technique. *Magn. Reson. Med.* **29,** 616–622 (1993).
7. R. Kuwatsuru, D. M. Shames, A. Muhler, J. Mintorovitch, V. Vexler, J. S. Mann, F. Cohn, D. Price, J. Huberty, R. C. Brasch, Quantification of tissue plasma volume in the rat by contrast-enhanced magnetic resonance imaging. *Magn. Reson. Med.* **30,** 76–81 (1993).
8. M. E. Moseley, W. M. Chew, D. L. White, J. Kucharczyk, L. Litt, N. Derugin, J. Dupon, R. C. Brasch, D. Norman, Hypercarbia-induced changes in cerebral blood volume in the cat: a ^{1}H MRI and intravascular contrast agent study. *Magn. Reson. Med.* **23,** 21–30 (1992).
9. M. S. Neuder, "A study of blood-brain barrier permeability variations *in vivo* using magnetic resonance imaging," Ph.D. Thesis, Massachusetts Institute of Technology, 1993.
10. K. M. Donahue, D. Burstein, W. J. Manning, M. L. Gray, Studies of Gd-DTPA relaxivity and proton exchange rates in tissue. *Magn. Reson. Med.* **32,** 66–76 (1994).
11. M. F. Wendland, M. Saeed, K. K. Yu, T. P. L. Roberts, K. Lauerma, N. Derugin, J. Varadarajan, A. D. Watson, C. B. Higgins, Inversion recovery EPI of bolus transit in rat myocardium using intravascular and extravascular gadolinium-based MR contrast media: dose effects on peak signal enhancement. *Magn. Reson. Med.* **32,** 319–329 (1994).
12. R. M. Judd, M. K. Atalay, G. A. Rottman, E. A. Zerhouni, Effects of myocardial water exchange on T_1 enhancement during bolus administration of MR contrast agents. *Magn. Reson. Med.* **33,** 215–223 (1995).
13. C. Hazlewood, D. Chang, B. Nichols, D. Woessner, Nuclear magnetic resonance transverse relaxation times of water protons in skeletal muscle. *Biophys. J.* **14,** 583–605 (1974).
14. H. C. Schwickert, T. P. L. Roberts, D. M. Shames, C. F. van Dijke, A. Disston, A. Muhler, J. S. Mann, R. C. Brasch, Quantification of liver blood volume: Comparison of ultra short TI inversion recovery echo planar imaging (ULSTIR-EPI), with dynamic 3D-Gradient recalled echo imaging. *Magn. Reson. Med.* **34,** 845–852 (1995).
15. P. Wedeking, C. H. Sotak, J. Telser, K. Kumar, C. A. Chang, M. F. Tweedle, Quantitative dependence of MR signal intensity on tissue concentration of Gd(HP-DO3A) in the nephrectomized rat. *Magn. Reson. Imaging* **10,** 97–108 (1992).
16. S. H. Koenig, M. Spiller, R. D. III. Brown, G. L. Wolf, Relaxation of water protons in the intra- and extracellular regions of blood containing Gd(DTPA). *Magn. Reson. Med.* **3,** 791–795 (1986).
17. W. Sobol, S. Jackels, R. Cothran, W. Hinson, NMR spin-lattice relaxation in tissues with high concentration of paramagnetic contrast media: evaluation of water exchange rates in intact rat muscle. *Med Phys.* **18(2),** 243–250 (1991).
18. A. C. McLaughlin, J. S. Leigh Jr, Relaxation times in systems with chemical exchange. *J. Magn. Reson.* **9,** 296–304 (1973).
19. C. P. Rose, C. A. Goresky, G. G. Bach, The capillary and sarcolemmal barriers in the heart: an exploration of labelled water permeability. *Circ. Res.* **41(4),** 515–533 (1977).
20. K. M. Donahue, "Studies of Gd-DTPA relaxivity and proton exchange rates in tissue with implications for MR imaging of regional myocardial perfusion," Ph.D. Thesis, Harvard-Massachusetts Institute of Technology, Cambridge, 1993.
21. W. H. Press, S. A. Teuolsky, W. T. Vetterling, W. T. Flannery, *in* "Numerical Recipes in C. The Art of Scientific Computing," 2nd ed., Cambridge University Press, New York, 1992.
22. A. A. Bogdanov Jr., R. Weissleder, H. W. Frank, A. V. Bogdanova, N. Nossif, B. K. Schaffer, E. Tsai, M. I. Papisov, T. J. Brady, A new macromolecule as a contrast agent for MR angiography: preparation, properties, and animal studies. *Radiology* **187,** 701–706 (1993).
23. W. R. Bauer, K. Schulten, Theory of contrast agents in magnetic resonance imaging: coupling of spin relaxation and transport. *Magn. Reson. Med.* **26,** 16–39 (1992).